The Astrophysical Journal Supplement Series, 172:284–294, 2007 September

THE EFFECTS OF ENVIRONMENT ON MORPHOLOGICAL EVOLUTION AT $0 < z < 1.2$ IN THE COSMOS SURVEY[1]

Peter Capak,[2] Roberto G. Abraham,[3] Richard S. Ellis,[2] Bahram Mobasher,[4]
Nick Scoville,[2] Kartik Sheth,[2,5] and Anton Koekemoer[4]
Received 2006 September 22; accepted 2007 March 23

ABSTRACT

We explore the evolution of the morphology-density relation using the COSMOS Advanced Camera for Surveys (ACS) and previous cluster studies. The Gini parameter measured in a Petrosian aperture is found to be an effective way of selecting early-type galaxies free from systematic effects with redshift. We find that galaxies are transformed from late- (spiral and irregular) to early-type (E+S0) galaxies more rapidly in dense than in sparse regions. At a given density, the early-type fraction grows constantly with cosmic time, but the growth rate increases with density as a power law of index 0.29 ± 0.02. However, at densities below 100 galaxies Mpc^{-2}, no evolution is found at $z > 0.4$. In contrast, the star formation–density relation shows strong evolution at all densities and redshifts, suggesting that different physical mechanisms are responsible for the morphological and star formation transformation. We show that photometric redshifts can measure local galaxy environment, but that the present results are limited by photometric redshift error to densities above $\Sigma = 3$ galaxies Mpc^{-2}.

Subject headings: cosmology: observations — galaxies: clusters: general — galaxies: evolution — galaxies: formation — galaxies: structure — large-scale structure of universe

1. INTRODUCTION

The correlation of galaxy properties such as color and morphology with galactic environment, specifically the local density of galaxies, was first noted by Hubble (1926). Later, low-redshift surveys showed a high percentage of early-type (E+S0) and redder galaxies in clusters compared with the field, which was quantified as the morphology-density (T-Σ) relation (Dressler 1980; Dressler et al. 1997; Treu et al. 2003; Smith et al. 2005; Postman et al. 2005) and the star formation rate–density (SFR-Σ) relation (Oemler 1974; Melnick & Sargent 1977; Butcher & Oemler 1984; Kauffmann et al. 2004). Spectroscopic redshifts from the Sloan Digital Sky Survey (SDSS) enabled an extension of these correlations over 5 orders of magnitude in Σ at $z \leq 0.1$ (Goto et al. 2003; Kauffmann et al. 2004). Such studies clearly indicate that the present properties of galaxies have been strongly influenced by galaxy environment, presumably by galaxy interactions.

Most investigations of galaxy evolution have focused on the star formation rates and stellar masses as determined from integrated photometry and spectroscopy (Cowie et al. 1999; Lilly et al. 1995; Dickinson et al. 2003; Glazebrook et al. 2004; Bauer et al. 2005; Drory et al. 2005; Feulner et al. 2005; Juneau et al. 2005). In these studies, star formation activity is seen to progress to less massive galaxies as the universe ages, a phenomenon often called "downsizing" (Cowie et al. 1999). Nevertheless, the process of star formation in galaxies is complex and poorly understood (Somerville 2005). On the other hand, the morphology of a galaxy is linked to the angular momentum distribution, which is simpler to quantify, and hence is a valuable alternative to star formation. The presence of a disk clearly indicates a dynamically cold stellar population that has not been significantly disturbed, while it is likely that spheroidal systems have been heated by interactions, merging, or other mechanisms.

At redshifts $z > 0.3$, ground-based imaging generally has inadequate resolution for morphological surveys, since the typical size of a galaxy is $\leq 0.75''$ (Ferguson et al. 2004); therefore, *Hubble Space Telescope* (*HST*) data are required. The small field of view available on *HST* limited previous studies of the T-Σ relation at $z > 0.3$ to a few previously known galaxy clusters and field samples (Dressler et al. 1997; Treu et al. 2003; Postman et al. 2005). Combining these studies, Smith et al. (2005) found that high- and low-density regions evolved differently. They postulated that different formation times were possibly responsible for the observed effect, but were limited by the look-back time and density resolution of the available data. The COSMOS Advanced Camera for Surveys (ACS) data are the first *HST* imaging survey data able to provide statistically significant samples of galaxies over a range of environments and redshifts with high-resolution morphologies.

In this paper, we use the COSMOS data, combined with photometric redshifts, to quantify the evolution of the T-Σ relation as a function of redshift over the range $z = 0.3$–1.2. These measurements are combined with previous studies in the literature (Dressler 1980; Dressler et al. 1997; Postman et al. 2005; Smith et al. 2005) to provide a larger dynamic range in density and span in redshift than possible with COSMOS data alone. In § 2, we describe the

[1] Based in part on observations with the NASA/ESA *Hubble Space Telescope*, obtained at the Space Telescope Science Institute, which is operated by the Association of Universities for Research in Astronomy (AURA), Inc., under NASA contract NAS5-26555; the Subaru Telescope, which is operated by the National Astronomical Observatory of Japan; the MegaPrime/MegaCam, a joint project of the Canada-France-Hawaii Telescope (CFHT) and CEA/DAPNIA, at the CFHT, which is operated by the National Research Council of Canada, the Institut National des Sciences de l'Univers of the Centre National de la Recherche, and the University of Hawaii; and Kitt Peak National Observatory, Cerro Tololo Inter-American Observatory, and the National Optical Astronomy Observatory, which is operated by AURA under cooperative agreement with the National Science Foundation.

[2] California Institute of Technology, Department of Astronomy, 105-24 Caltech, Pasadena, CA 91125.

[3] Department of Astronomy and Astrophysics, University of Toronto, 60 St. George Street, Room 1403, Toronto, ON M5S 3H8, Canada.

[4] Space Telescope Sciences Institute, 3700 San Martin Drive, Baltimore, MD 21218.

[5] Spitzer Science Center, California Institute of Technology, 220-6 Caltech, Pasadena, CA 91125.

TABLE 1
NUMBER OF OBJECTS IN REDSHIFT BINS

Redshift Range	F814W < 24	$M_V \leq -21.2$–Look-back Time
$0.2 < z \leq 0.4$	18250	2154
$0.4 < z \leq 0.6$	17419	2817
$0.6 < z \leq 0.8$	27018	6193
$0.8 < z \leq 1.0$	19062	7829
$1.0 < z \leq 1.2$	13075	7799
$1.2 < z \leq 1.4$	7975	6166

imaging data and photometric redshifts (Mobasher et al. 2007) used for this study and the selection of our sample. The morphological parameters used to characterize the galaxies are discussed and tested in § 3. Details of estimating density with photometric redshifts and correspondingly poor line-of-sight distances are discussed in § 4. Finally, the dependence of morphology on density and redshift is presented and discussed in §§ 6 and 7, respectively. Throughout this paper we use a standard cosmology with $\Omega_v = 0.7$, $\Omega_m = 0.3$, and $H_0 = 75$ km s^{-1} Mpc^{-1}. All literature values are converted to this cosmology unless otherwise noted.

2. IMAGING AND REDSHIFTS

The *HST* ACS images, taken as a part of the COSMOS survey (Scoville et al. 2007b; Koekemoer et al. 2007) are used to measure morphologies. These images cover an area of $\sim$1.8 deg^2 in F814W and 81 arcmin^2 in F475W with single-orbit exposures. The completeness is 50% in F814W for a galaxy 0.5″ in diameter with $F814W_{AB} = 26$ mag (Scoville et al. 2007b). The point-source depth is $\sim$2 mag deeper, but this is not relevant to morphological studies. The median image quality is 0.05″ and 0.08″ (FWHM) in F475W and F814W, respectively.

Photometric redshifts are determined from multiband ground-based photometry (Capak 2007) as described in Mobasher et al. (2007). Our present investigation is focused on redshifts $z = 0.3$–1.2, for which the photometric redshifts have an accuracy $\sigma_z/(1+z) = 0.03$ for galaxies with $I_{AB} < 24$ mag. The redshift accuracy was determined directly by comparison of the photometric redshifts with spectroscopic redshifts for over 900 galaxies at $z < 1.2$ with $I_{AB} < 24$ mag in the COSMOS field.

A magnitude cutoff of F814W < 24 mag was adopted based on experimentation in making morphological measurements. Below this magnitude, the low surface brightness also leads to incompleteness for a typically sized $z = 1$ galaxy, which is 0.75″ in size (Ferguson et al. 2004; Scoville et al. 2007b).

Stars are removed from the object catalog using the SExtractor (Bertin & Arnouts 1996) `CLASS_STAR` parameter measured on the ACS F814W image. Objects with `CLASS_STAR` ≥ 0.9 are considered to be stars.

A total of 120,187 galaxies meet our magnitude cut of F814W < 24 mag and fall outside of the masked regions on the images. Of these, 32,958 meet the criteria to be used in our morphology-density analysis (see §§ 4 and 6). Table 1 gives the number of objects as a function of redshift.

3. MORPHOLOGICAL CLASSIFICATION

Galaxies exhibit a range of morphologies and are difficult to quantify automatically. Therefore, classification by eye is often used to test the efficacy of automated classifiers. At high redshifts two additional problems arise: surface brightness dimming [$\propto (1+z)^4$] reduces the visibility of disk-identifying features such as arms and bars, and redshifting (or band shifting) means that the observed visible bands increasingly sample the rest-frame ultraviolet (UV). The UV is unlikely to provide a reliable classification of the major galactic stellar components, since it is highly biased in favor of the youngest star-forming regions and areas of low extinction. These redshift-dependent effects introduce systematics which are difficult to separate from the desired evolutionary trends.

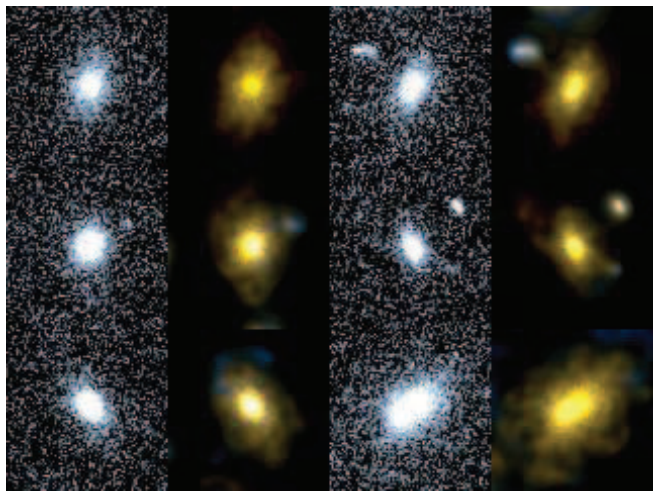

FIG. 1.—Six galaxies with early-type visual classifications and late-type automated classification. The gray-scale images are the F814W images used for the visual classification with a square root stretch. The color images have the same stretch and cuts, but are made from the *HST* ACS F475W and F814W images which were adaptively smoothed using the method described in Scoville et al. (2007a). Notice the low surface brightness features obvious in the color images, but hidden in the gray-scale images.

Most of the automated morphological classification schemes (Abraham et al. 1994, 1996; Conselice et al. 2003) have focused on separating elliptical, disk, and irregular systems; these galaxies exhibit a wide variety of structure, and their appearances are very dependent on viewing angle and other projection effects. On the other hand, dynamically hot systems (E+S0 galaxies) are generally more centrally concentrated (therefore less susceptible to surface brightness dimming) and more spherical (therefore less subject to projection effects). Thus, many difficulties in the morphological classification discussed above can be minimized by selecting just the early-type (E+S0) population. Specifically, independent of the method, we classify galaxies with respect to whether or not they are early-type, and do not differentiate within the late-type population. This binary classification is entirely adequate for studying the T-Σ relation, so long as any systematic biases do not vary with redshift or density.

Surface brightness has proven particularly problematic for previous morphological studies (R. Ellis & R. Abraham 2006, private communication). Both visual and automated classification schemes miss low surface brightness disks, resulting in systematic effects with magnitude and redshift. These systematic effects can be mitigated by defining the edge of an object in a way which is independent of signal-to-noise ratio per pixel. Figure 1 illustrates one such method for eyeball classifications. The original *HST* ACS F814W images are shown together with adaptively smoothed images for several galaxies with faint disks, all of which were visually classified as early types (Scoville et al. 2007a). The stretch and scale factors are identical for all images. The adaptive smoothing gives equal signal-to-noise ratio per resolution element, but with varying spatial resolution dependent on the local signal-to-noise ratio (i.e., with higher resolution in brighter areas). This enhances the visibility of low surface brightness, extended features. In the processed images, spiral structure becomes visible

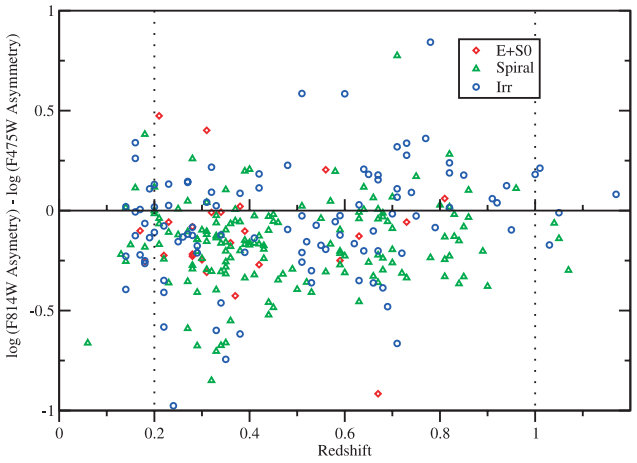

FIG. 2.—Difference between log (asymmetry) measured in F475W and F814W vs. redshift. Notice the systematic trends with redshift as the two bands go from sampling the rest-frame optical to the rest-frame UV. Clumps of active star formation are more visible in the rest-frame UV, increasing the measured asymmetry. This transition happens at $z \simeq 0.2$ for F475W and $z \simeq 1.0$ for F814W. These transitions are indicated with dotted lines.

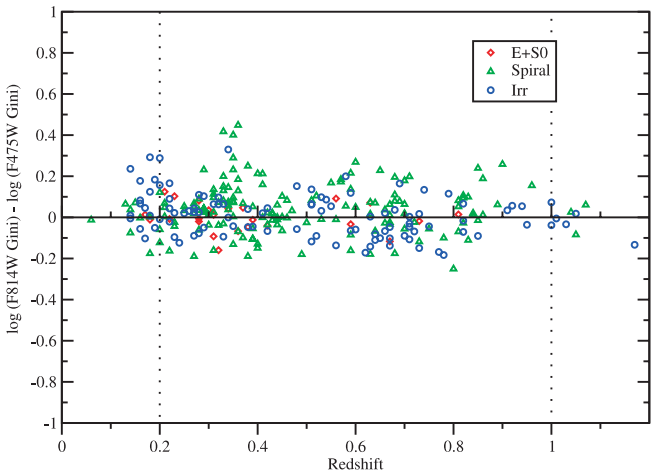

FIG. 3.—Difference between log (Gini) measured in F475W and F814W vs. redshift. Notice there are no systematic trends with redshift as the two bands go from sampling the rest-frame optical to the rest-frame UV. The transition from optical to UV light happens at $z \simeq 0.2$ for F475W and $z \simeq 1.0$ for F814W. These transitions are indicated with dotted lines.

in all four galaxies, although it was difficult to see visually in the original images.

Petrosian apertures provide object limits (edges) independent of signal-to-noise ratio per pixel for automated classification methods (Lotz et al. 2004). We use a "quasi-Petrosian" aperture to minimize the effects of surface brightness dimming. This was constructed using a new algorithm that is intended to work for galaxies of arbitrary shape, and which has more graceful convergence properties than the usual formulation of Petrosian apertures. (Ordinary Petrosian indices are based on circular apertures and are not guaranteed to converge.) The details of our procedure are given in Abraham et al. (2007), and only an outline is given here. The first step is to use SExtractor to isolate the galaxy from the sky. The flux values of the pixels in the galaxy are then sorted in decreasing order to construct a curve of sorted flux values. This curve is then summed over to construct a curve of cumulative flux values, which is then multiplied by a scale factor η. The flux value at which the scaled cumulative distribution intersects the sorted pixel value distribution defines a critical flux value. Only those pixels with fluxes greater than this critical value are used in calculating the "quasi-Petrosian" coefficients.

Rotational asymmetry and Gini are two commonly used parameters for automated morphological classification (Abraham et al. 1994, 1996; Conselice et al. 2003). The asymmetry coefficient is calculated from the difference between the galaxy image and its image rotated 180° about its central peak. The Gini parameter measures segregation of light into bright and faint pixels and is strongly correlated with the concentration of galaxy light, but the Gini parameter is a more robust indicator of galaxy morphology than the usual concentration coefficient (Abraham et al. 2003). In particular, Gini is less sensitive to surface brightness effects and does not require a well-defined centroid. Specific details of our Gini and asymmetry measurements are given in Abraham et al. (2007).

The *HST* F814W data, which covers the whole field, will sample a different rest-frame wavelength range at each redshift. Therefore, any morphological classification scheme used to study galaxy evolution must be independent of the rest-frame wavelength. We can test for systematic variations due to band shifting in our data by using the central 81 arcmin^2 of COSMOS with dual band coverage (F814W and F475W). Figure 2 shows the difference between asymmetry measured in the F475W and F814W bands with redshift. A shift between the classifications derived in the two bands is observed at $z \sim 0.2$, where the median wavelength of the F475W band moves into the rest-frame UV light, while F814W still samples the rest-frame visible. A shift back to consistent classification occurs at $z \sim 1.0$, where both bands sample the rest-frame UV light. As noted earlier, the rest-frame UV selects regions of active star formation, which tend to be irregular and/or clumpy; as a result, the asymmetry is significantly higher in the rest-frame UV than in the rest-frame optical. Figure 3 shows the difference between Gini measured in the F475W and F814W bands with redshift. The scatter is much smaller, and no systematic trends with redshift are observed.

Figure 4 shows a version of the Abraham et al. (1996) morphology classification system compared to visual morphologies. Visual morphologies were provided by one of us (R. S. E.) for a complete sample of $\simeq$2000 F814W < 22.5 mag galaxies in the inner, dual-band coverage region using the precepts discussed in Bundy et al. (2005). The scatter is reasonably large due to the effects of band shifting and surface brightness dimming on the asymmetry coefficient and visual classification. The difference between spiral and irregular galaxies is not important for the present investigation of the T-Σ relation; we therefore use only the Gini parameter to classify early-type galaxies. We chose a cut at $\log(\mathrm{Gini}) \leq -0.35$ as the dividing line between early- and late-type galaxies because it gave a similar fraction of early- and late-type galaxies as the Abraham et al. (1996) system at $0.2 \leq z \leq 0.4$. Figure 5 shows a region of Figure 4 near the division line between early- and late-type galaxies. The axes are identical, but the symbols have been replaced with color images of the actual galaxies. Our specified cut in the Gini coefficient clearly separates early- and late-type galaxies.

4. DENSITY ESTIMATE

We adopted the *N*th neighbor projected density estimate introduced by a number of previous investigators (Dressler 1980; Dressler et al. 1997; Postman et al. 2005; Smith et al. 2005). The projected density in the vicinity of each galaxy is estimated from the distance to the *N*th neighbor. This distance defines the

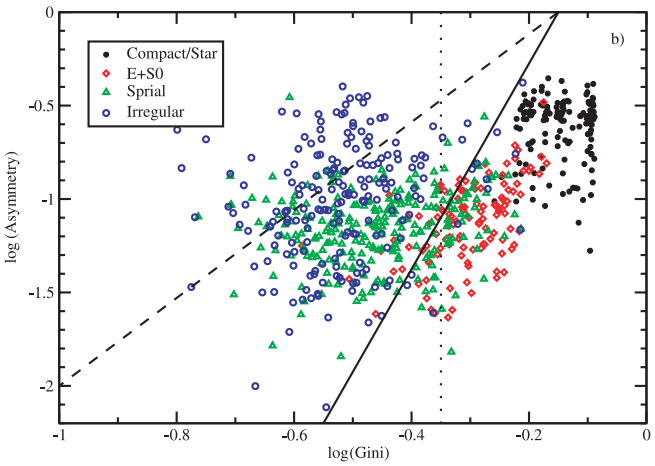

FIG. 4.—Comparison of qualitative and quantitative morphologies. Morphological parameters measured from the *HST* F814W images are plotted for objects with visual morphological classification. The Gini parameter and rotational asymmetry measured in a Petrosian aperture are plotted for objects with visual classifications. Dividing lines are drawn between regions of predominantly irregular, spiral, and elliptical types. The dashed line between irregular and spiral galaxies is defined as log (asymmetry) = 2.353 log (Gini) + 0.353, while the solid line between spiral and early-type galaxies is defined as log (asymmetry) = 5.500 log (Gini) + 0.825. The dotted line is a cut at log (Gini) = 0.35, used to select early-type galaxies in this paper. This selection gives an equivalent fraction of early-type galaxies as the Gini-asymmetry selection at $0.2 \leq z \leq 0.4$. Stars and very compact objects appear in the upper right of this plot, but are removed in our later analysis.

radius of a circle whose area is used to estimate the surface density as

$$\Sigma = \frac{N}{\pi r^2}. \tag{1}$$

To be consistent with previous studies, we chose to use the 10th nearest neighbor. A median background density is then subtracted to correct for line-of-sight superposition due to uncertainties in the distances (i.e., redshift). This estimator is optimal when line-of-sight distances are uncertain, since only projected distances need to be estimated.

Photometric redshifts improve the nearest neighbor method in several key ways. The rest-frame absolute luminosity of galaxies can be accurately estimated so that similar galaxies (from the same part of the luminosity function) can be selected at all redshifts. The nearest neighbor counting can be done in redshift bins rather than along the entire line of sight, reducing the background contamination and allowing multiple structures to be discriminated in the same field. In addition, the reduction in background galaxy counts enables one to probe to much lower projected densities.

Following Smith et al. (2005), we adopt a luminosity cut of $M_V \leq -21.2$ mag at $z = 1$ and allow for 1 mag of passive evolution between $z = 1$ and the present. This should select a similar mix of galaxies at all redshifts. Furthermore, maintaining a consistent magnitude cut between studies is very important because the galaxy density and morphological mix may change with magnitude (Benson et al. 2001).

With this magnitude cut and fading due to band shifting, our F814W data are sufficiently deep at $z \leq 1.4$; however, a redshift slice of $\pm 3\,\sigma_z$ is required around each galaxy to ensure all objects in a structure are measured. As a result, we are only able to accurately measure densities for $z \leq 1.3$.

4.1. *Accuracy of the Density Estimator*

The accuracy of the photometric redshifts determines the minimum density to which the *n*th nearest neighbor method will work. This minimum density can be estimated by considering a structure of density Σ_s embedded in a random background of density $\rho_{\rm bkg}$, where $\rho_{\rm bkg}$ is the number density of galaxies per Mpc^2 per redshift interval. The projected density of background sources for a slice of thickness Δz along the line of sight is then $\Sigma_{\rm bkg} = \rho_{\rm bkg}\Delta z$. Assuming that Δz is large enough to include all galaxies within the structure, the fraction of galaxies actually in the structure is given by

$$F_{\rm real} = \frac{\Sigma_s}{\Sigma_s + \Sigma_{\rm bkg}} = \frac{\Sigma_s}{\rho_{\rm bkg}\Delta z + \Sigma_s}. \tag{2}$$

Equation (2) can also be inverted to define a minimum density above which a certain fraction of the galaxies will be members of a given structure. We do not need to consider Poisson error because Σ is determined with the same number of galaxies at all densities.

In the present data, the largest redshift error is at $z = 1.3$, where $\sigma_z = 0.065$ and $\Sigma_{\rm bkg} = 3$ Mpc^2. This means 50% of galaxies will be assigned to the correct structures at $\Sigma_s = 3$ Mpc^2, and 77% will be correctly assigned at $\Sigma_s = 10$ Mpc^2. At $z = 0.3$, $\sigma_z = 0.036$ and $\Sigma_{\rm bkg} = 4$ Mpc^2, so 42% of galaxies will be assigned to the correct structures at $\Sigma_s = 3$ Mpc^2, and 71% will be correctly assigned at $\Sigma_s = 10$ Mpc^2.

4.2. *Relation of Σ to Volume Density*

Ideally, one would measure volume densities rather than projected densities. Unfortunately, the line-of-sight error from photometric redshifts make volume densities difficult to measure (Cooper et al. 2005). To first order, the relation between the projected mean density, $\bar{\Sigma}$, and volume density is

$$\bar{\rho} = \frac{3\bar{\Sigma}}{4r} = \sqrt{\frac{9\pi}{16N}}\bar{\Sigma}^{3/2} = 0.42\bar{\Sigma}^{1.5} \tag{3}$$

if we assume spherical symmetry.

To see how well this relation holds, we created a simulated galaxy catalog with structures of known density. The structures had a Gaussian density profile and peak densities ranging from 1 to 300 galaxies Mpc^{-3}, similar to the observed range in COSMOS. The results are shown in Figure 6*a*. There is a strong correlation between the input and recovered densities for all but the sparsest regions (below $\Sigma \simeq 3$ galaxies Mpc^{-2}), where our assumption of spherical symmetry breaks down. Furthermore, the same assumption appears to overestimate the true density by a factor of $\sim$2–3. This is also due to our assumption of spherical symmetry, which will underestimate the true volume. This offset is only applicable if projected densities used in this paper are converted to real space densities. No offset is observed between projected densities measured with and without redshift error.

In addition to these effects, objects in low-density regions projected in front of or behind a dense region are scattered to higher densities; however, the fraction of these objects is less than 2% of the total, and can be neglected. Figure 6*b* shows the effect of redshift error on the density analysis. The scatter is larger than in Figure 6*a* due to the line-of-sight errors; however, the real space density is clearly recoverable.

Similar tests by Cooper et al. (2005) on mock galaxy catalogs from cold dark matter (CDM) simulations agree with our results (see Table 2 and Fig. 1 in Cooper et al. 2005). However, the

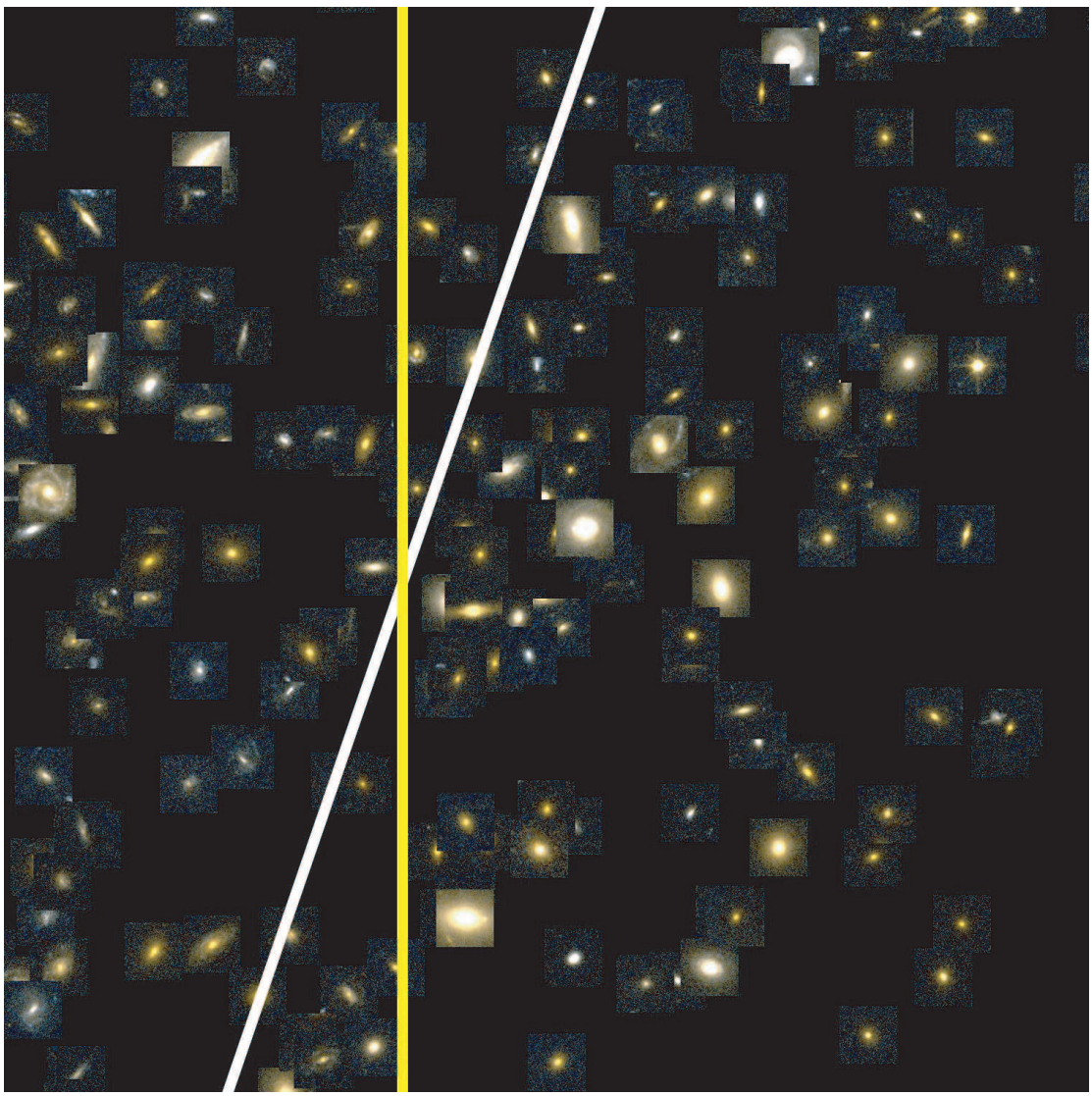

FIG. 5.—Magnified region of Fig. 4 around the division of early- and late-type galaxies. The points are replaced with color images of the classified objects. The white line corresponds to the division of early- and late-type galaxies in Gini and asymmetry, while the yellow line is our cut at log (Gini) = 0.35. Notice the clear division of early- and late-type galaxies by our cut in Gini (*yellow line*).

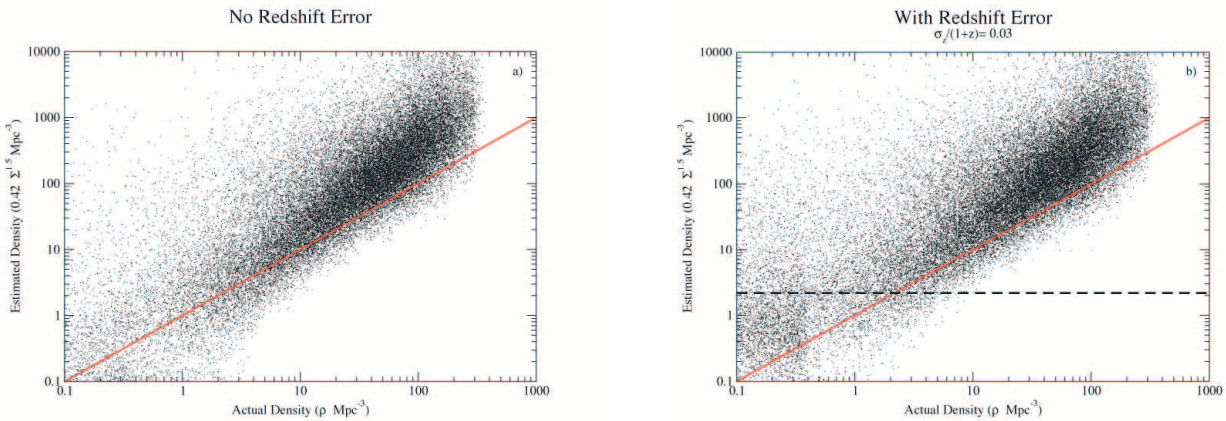

FIG. 6.—Comparison of real-space and projected density estimates for a simulated catalog with structures of known density. Panel *a* includes no redshift error, while panel *b* includes a redshift error of $\sigma_z/(1+z) = 0.03$. The dashed line in panel *b* indicates the minimum measurable density, $\Sigma = 3$, estimated by eq. (2). A clear correlation is seen between the actual and projected densities over several orders of magnitude.

TABLE 2
PARAMETERS OF PREVIOUS T-Σ STUDIES

Reference	Redshift Range	H_0 (km s^{-1} Mpc^{-1})	Ω_m	Ω_V	Magnitude Limit[a]	Correction to Density[b]	Correction to F_{E+S0}
Dressler (1980)	0.011–0.066	50	1.0	0.0	−19.75	−0.33	0.0
Goto et al. (2003)	0.05–0.1	75	0.3	0.7	−20.3[c]	0.0	0.0
Dressler et al. (1997)	0.37–0.56	50	1.0	0.0	−20.0	−0.47	−0.045
Treu et al. (2003)	0.4	65	0.3	0.7	−18.7	−0.38	−0.056
Smith et al. (2005)	0.78–1.27	65	0.3	0.7	−21.2[d]	−0.12	0.0
Postman et al. (2005)	0.4–1.27	70	0.3	0.7	−20.07[d]	−0.32	−0.045

[a] The values given represent the upper limit of M_V in an $H_0 = 75$ km s^{-1} Mpc^{-1}, $\Omega_m = 0.3$, $\Omega_V = 0.7$ cosmology.
[b] In units of logΣ. The correction includes conversion to a $H_0 = 75$ km s^{-1} Mpc^{-1}, $\Omega_m = 0.3$, $\Omega_V = 0.7$ cosmology and an offset for the different magnitude limits.
[c] The actual limit is $M_r \leq -20.5$, which corresponds to $M_V \leq -20.3$ at the median galaxy color.
[d] The values given are for $z = 1$; Smith et al. (2005) allows for 1 mag of passive evolution between $z = 1$ and $z = 0$, while Postman et al. (2005) allows for 0.8 mag of passive evolution.

average density in the COSMOS data is significantly higher than those in the Cooper et al. simulations, which leads Cooper et al. to conclude that the accuracy of photometric redshifts is not sufficient for the majority of galaxies. A density of $\Sigma = 10$ galaxies Mpc^{-2} corresponds to $\log(D_5) = -0.16$ in Cooper et al., above which there are very few galaxies in their simulation, but a significant number of galaxies in the COSMOS data.

To understand these differences, we applied our estimator to mock galaxy catalogs provided by the Millennium Simulation (Springel et al. 2005). These are the same simulations used by Cooper et al., but with dimensions and limiting magnitudes for the COSMOS survey. As found by Cooper et al., densities above $\Sigma = 3$ galaxies Mpc^{-2} are successfully measured with photometric redshifts. However, the number of galaxies at densities greater than 3 galaxies Mpc^{-2} in the Millennium Simulation is considerably lower than that from the COSMOS data. Figure 7 shows the distribution of densities recovered from the Millennium Simulation and from the COSMOS survey. At densities $\Sigma > 3$ there are a factor of ∼10 more galaxies in the COSMOS survey than in the v2.0 simulations.

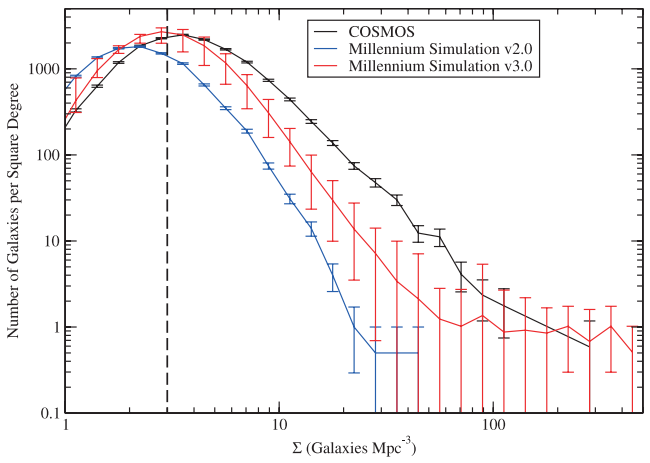

FIG. 7.—Density distribution of galaxies for $0.2 < z < 1.2$. The number of galaxies per unit area at each density are shown for COSMOS and mock catalogs from two versions of the Millennium Simulation (Springel et al. 2005). The vertical dashed line indicates the minimum measurable density, $\Sigma = 3$, estimated by eq. (2). The v2.0 mock catalog populates the dark matter halos in a way similar to those used in Cooper et al. (2005), while the v3.0 mock catalog follows galaxy orbits in detail. The selection function, redshift error, and area of the simulations are identical to the COSMOS data. Notice that the distribution of densities in the v2.0 mock catalog is significantly lower than in the actual data. Error bars indicate the measurement Poisson error except for the v3.0 mock catalog, which also includes the expected range of cosmic variance.

The discrepancy in density distribution is due to the way in which galaxies are distributed within dark matter halos. In earlier versions of the Millennium Simulation, galaxy orbits were not followed in detail after dark matter halos merged (M. Kitzbichler & S. White 2006, private communication). This resulted in systematically fewer galaxies in high-density regions. This has been corrected in the latest versions (v3.0 and newer) of the simulation, improving the agreement, but still underestimating the number of galaxies in high-density regions (see Fig. 7). However, McCracken et al. (2007) find a higher amplitude in both the overall correlation function and the correlation function on small scales than predicted by the mock catalogs, which indicates that the mock catalogs still tend to underpopulate dense regions.

5. COMPARISON WITH LITERATURE DATA

It is important to maintain a consistent magnitude limit when studying the morphology-density relation because the galaxy density and morphological mix may change with magnitude (Benson et al. 2001) (see § 4). Dressler (1980), Dressler et al. (1997), Postman et al. (2005), and Treu et al. (2003) use a magnitude limit more than a magnitude fainter than Goto et al. (2003), Smith et al. (2005), and this paper (see Fig. 8). To quantify the effects of the different limiting magnitudes in the literature, we began by

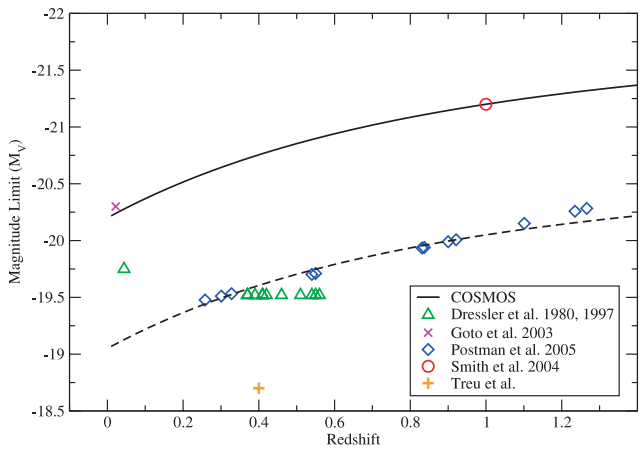

FIG. 8.—Limiting magnitude for various studies of the T-Σ relation along with the limit used in this sample (*solid line*). The Goto et al. (2003) point has been converted from M_r to M_V assuming the median rest-frame color observed in the COSMOS data for $0.2 < z < 0.4$ [$(V - r) = 0.2$]. Dressler (1980), Dressler et al. (1997), and Postman et al. (2005) use a limiting magnitude 1 mag fainter than our study. The dashed line indicates a limiting magnitude of $M_V < -19.05$ with 1 mag of passive evolution.

constructing morphologically selected luminosity functions uncorrected for incompleteness at the faint end. These are shown for five redshift bins in Figure 9. The solid lines mark our magnitude limit, while the dashed lines indicate the fainter limit used by Dressler (1980), Dressler et al. (1997), and Postman et al. (2005). A dotted line (*top panel*) in the $0.2 < z < 0.4$ bin indicates the limit used by Treu et al. (2003). The overall fraction of late-type galaxies is clearly higher at fainter magnitudes. In addition, our data become incomplete at $z > 0.8$ for the fainter magnitude limits.

We estimate corrections for the differing magnitude limits by analyzing our data with three magnitude limits at $z = 1$: $M_V \leq -21.2$ mag, $M_V \leq -20.05$ mag, and $M_V \leq -19.05$ mag. All three analyses include 1 mag of passive evolution between $z = 1$ and the present. The $M_V \leq -20.05$ mag limit corresponds to Dressler et al. (1997) and Postman et al. (2005), while $M_V \leq -19.05$ mag matches the Treu et al. (2003) work at $z = 0.4$.

The density measured with both fainter magnitude limits is 0.26 dex higher than that measured with $M_V \leq -21.2$ mag at densities $\Sigma > 3$ galaxies Mpc^{-2}. This offset appears to vary with density at $\Sigma < 3$ galaxies Mpc^{-2}. However, these densities are not reliable (see § 4.1), and the trend is not apparent at higher densities. No trend with redshift was observed in either magnitude bin or at any density.

The early-type fraction is 0.045 lower using a limit of $M_V \leq -20.05$ mag, and 0.056 lower with a limit of $M_V \leq -19.05$ mag than with a limit of $M_V \leq -21.2$ mag. No significant trends in these offsets are observed with density between 3 and 100 galaxies Mpc^{-2} or redshift between 0.2 and 0.8. However, we do not probe the highest densities and redshifts used in the literature.

A summary of the literature data and the correction factors applied is given in Table 2.

6. RESULTS

Our measurements of the T-Σ relation, along with those taken from the literature (Dressler 1980; Dressler et al. 1997; Goto et al. 2003; Smith et al. 2005; Postman et al. 2005), are shown in Figure 10 for five redshift bins. The densities for the literature points have been converted to an $\Omega_v = 0.7$, $\Omega_m = 0.3$, $H_0 = 75$ km s^{-1} Mpc^{-1} cosmology and corrected for differences in the limiting magnitude. After applying these corrections, our data are consistent with the earlier studies. The COSMOS data significantly improve the precision of the early-type morphological fraction, and increase the redshift and density resolution compared to earlier studies. We find that the T-Σ relation was already in place at $z > 1$, but differs from the local relation. As seen in previous studies (Postman et al. 2005; Smith et al. 2005), the early-type fraction is smaller and increases more gradually with density at $z = 1$ than at $z = 0$. This same redshift evolution is seen in a similar but independent analysis of the COSMOS data in Guzzo et al. (2007) and Cassata et al. (2007).

The evolution of the T-Σ relation with redshift is encapsulated in Figure 11. This figure shows the fraction of early-type galaxies as a function of time for four different density bins; growth in the early-type fraction with look-back time is seen at all densities, with more rapid growth at higher densities. However, the majority of the evolution occurs at $z < 0.4$ for densities below ~100 galaxies Mpc^{-2}. Assuming the growth rate of the early-type fraction is smooth, a line can be fit to the data at each density bin in Figure 11. The slope of this line yields the growth rate of the early-type fraction at any given density; the lines are plotted in Figure 12.

Figure 12 shows a clear trend for more rapid early-type (E+S0) production at higher densities. The data are well fit by a power

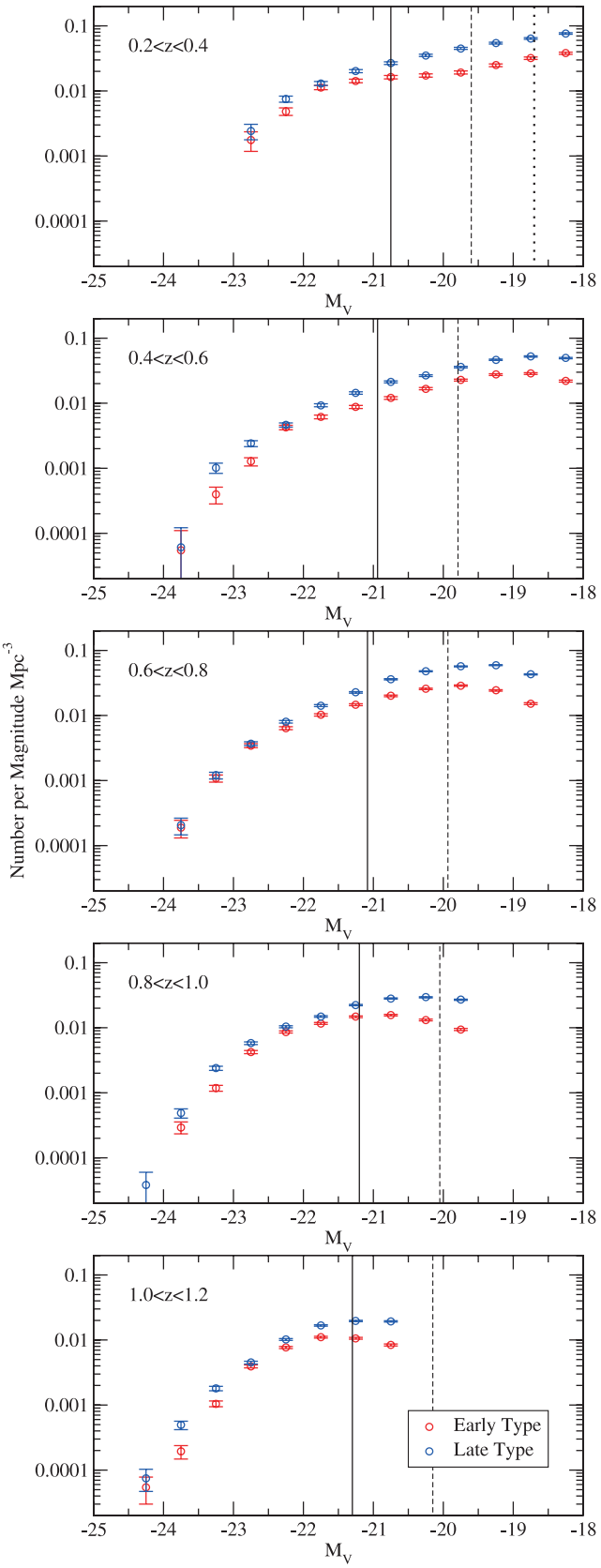

FIG. 9.—Luminosity function of galaxies in COSMOS split by morphological type for five redshift bins. These are uncorrected for incompleteness. The solid lines mark our absolute magnitude limit; the dashed line indicates the fainter limit used by Dressler (1980), Dressler et al. (1997), and Postman et al. (2005); and the dotted line in the top panel indicates the limit used by Treu et al. (2003). Notice the larger fraction of late-type galaxies at fainter magnitudes and the fact that our data become incomplete at $z > 0.8$ for the fainter absolute magnitude limit.

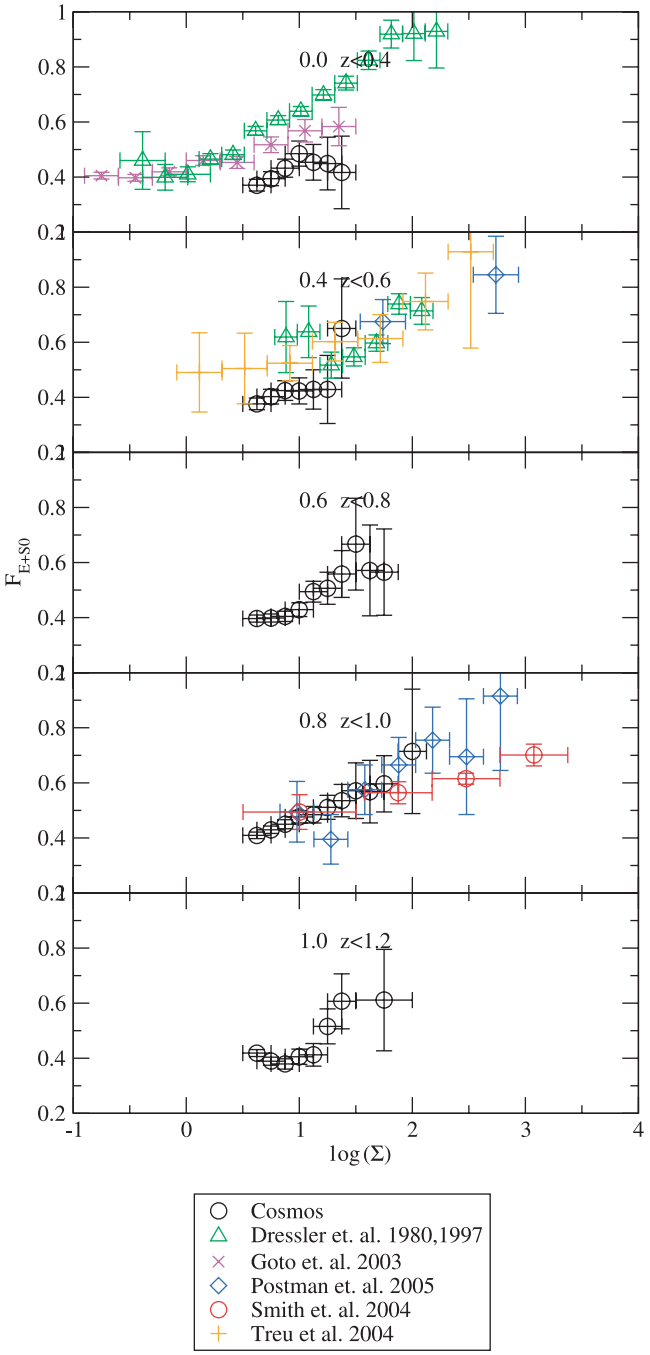

FIG. 10.—Elliptical fraction by density and redshift. The morphology-density relation is shown for five redshift intervals, $0.2 \leq z < 0.4$, $0.4 \leq z < 0.6$, $0.6 \leq z < 0.8$, $0.8 \leq z < 1.0$, and $1.0 \leq z < 1.2$, along with results from similar studies. The literature values have been converted to a cosmology with $\Omega_v = 0.7$, $\Omega_m = 0.3$, and $H_0 = 75$ km s^{-1} Mpc^{-1} and corrected for differences in the limiting magnitude of the samples. Note the increase in the elliptical fraction with density and decreasing redshift. These results agree with those of Dressler (1980), Dressler et al. (1997), Goto et al. (2003), and Postman et al. (2005). The lowest-density point from Smith et al. (2005) is discarded due to its large redshift error (see § 4.1).

law with a slope of 0.29 ± 0.02. However, without the $z < 0.4$ points, the growth rate drops off quickly at densities below $\sim$100 galaxies Mpc^{-2}. It should be noted that points with $\Sigma \geq 100$ galaxies Mpc^{-2} come entirely from cluster surveys in the literature. However, it is unlikely that the observed evolution is due to systematic effects, because all three studies (Treu et al. 2003; Smith et al. 2005; Postman et al. 2005) at these redshifts and densities use the same visual morphological classification system, and the trend to stronger evolution at higher density is seen by both Smith et al. (2005) and Postman et al. (2005) independently.

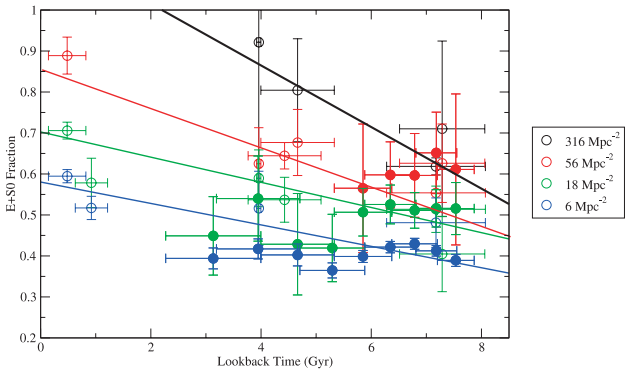

FIG. 11.—Evolution of the elliptical fraction with redshift for four densities. Notice the increased rate of elliptical formation with increased density and the lack of evolution at $z > 0.4$ in the lowest two density bins. Open points are a compilation from Dressler (1980), Dressler et al. (1997), Treu et al. (2003), Goto et al. (2003), Postman et al. (2005), and Smith et al. (2005); filled points are those from this study; and the lines are best fits to the data.

The growth in the fraction of non-star-forming (passive) galaxies is shown in Figure 13 along with the data from Figure 12. The spectral types are drawn from a similar analysis in Scoville et al. (2007a); however, the density measure and magnitude limit are the same ones used in this study, not those from Scoville et al. (2007a). Note the difference between the evolution measured from star formation and from morphology.

Many bulge-dominated but elongated objects with higher asymmetry (seen near the top of Fig. 4) are selected by both the Abraham et al. (1996) and our early-type selection. These elongated objects are likely edge-on S0 galaxies. The Gemini Deep Deep Survey (GDDS) finds that many of these elongated objects have residual star formation (Abraham et al. 2004). Although such objects with active star formation activity do not strictly meet the

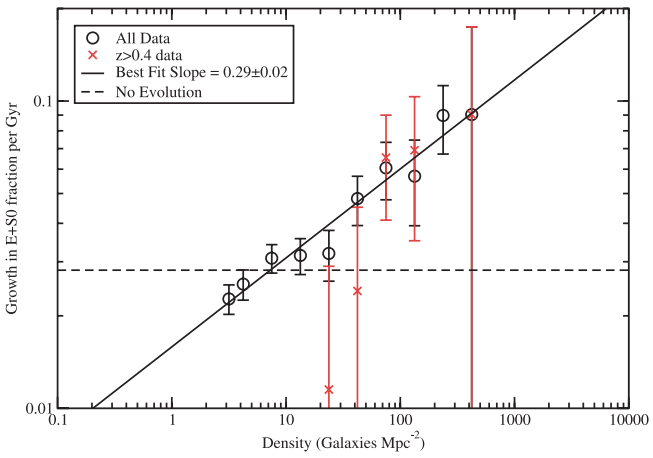

FIG. 12.—Growth rate of the E+S0 fraction as a function of density. The thick solid line is the best-fit power law to the data with a slope of 0.29 ± 0.02, while the dashed line shows the expected trend for no change in evolution rate with density. The red points indicate the measured evolution if only data at $z > 0.4$ are used. No evolution is observed at densities below $\Sigma < 100$ galaxies Mpc^{-2} at these high redshifts. These rates are derived from all data presented in Fig. 10, not the selected densities plotted in Fig. 11.

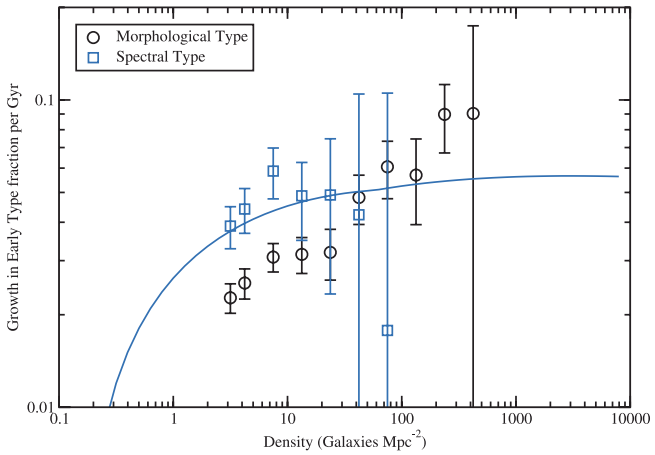

FIG. 13.—Growth rate in the non-star-forming (passive) galaxy fraction (*blue*), shown along with the growth rate in the early-type morphological fraction (*black*) as a function of density. The measured rates assume the growth rate is linear with time. The thick solid line is the linear growth rate expected by the best-fit closed-box model (eqs. [5] and [6]) at the weighted mean look-back time of the COSMOS data (6.5 Gyr). The best-fit model has $\eta = 1.07\Sigma^{0.08}$ and $t_0 = -0.99 \log \Sigma + 1.77$ Gyr. Notice the growth in the non-star-forming galaxy fraction is well fit by the closed-box model; however, no reasonable set of parameters can fit the growth in the morphological fraction unless more early types are intrinsically formed in dense regions.

criteria of early-type galaxies, they are bulge dominated, and hence more dynamically relaxed than galaxies with smaller Gini coefficients. These objects are likely progenitors of S0's or galaxies with early-type morphology undergoing a burst of star formation. Furthermore, since our Gini parameter is invariant with redshift, the same fraction of the galaxy population will be selected at all redshifts, implying that any contamination will not affect the observed evolution.

However, it is important to remember that there are multiple subclasses of early-type galaxies, and each subclass could be evolving differently. Postman et al. (2005) investigate this effect by analyzing the ellipticity distribution of cluster early-type galaxies and find no evolution in the ellipticity distribution between $z \simeq 1$ and $z \simeq 0.6$. A similar analysis of our data for $\Sigma > 10$ galaxies Mpc^{-2} also finds no evolution in the ellipticity distribution of early types. A Kolmogorov-Smirnov test finds that the distribution of ellipticities at $0.2 < z < 0.4$ is consistent with those at $0.8 < z < 1.2$ with 96.5% certainty. Therefore, any differential evolution in the E and S0 population is not seen in the overall ellipticity distribution of early-type galaxies.

7. DISCUSSION

Whether the morphology-density (T-Σ) relation is an intrinsic property of cluster galaxies or a result of environmental influence has been a matter of debate for some time. In contemporary simulations of galaxy formation, the majority of galaxies begin as dynamically cold, gas-rich, star-forming disks. They are subsequently transformed into early-type systems through interactions with other galaxies or by losing or exhausting the gas required to form stars. In this context there are two hypotheses explaining the T-Σ relation: that dense regions formed earlier than sparse ones, and that dense regions have stronger and more frequent interactions. A third hypothesis is that dense regions intrinsically form a higher fraction of early types, and that no transformation is needed.

The relative importance of these hypotheses can be distinguished with a simple closed-box model. If galaxy clusters were closed systems, one would expect the growth in the early-type fraction to slow with time as the fraction of early-type galaxies increases. This occurs because there are fewer late-type galaxies left to transform as the early-type fraction approaches 100%. Formally, the growth rate is given by

$$\frac{dN_{\rm E+S0}}{dt} = \left(1 - \frac{N_{\rm E+S0}}{N}\right) N\eta(\Sigma), \tag{4}$$

where the rate of change in the number density of early-type galaxies $N_{\rm E+S0}$ is given by the total number density of galaxies N and the conversion rate of late- to early-type galaxies per unit time as a function of density, $\eta(\Sigma)$. Integrating equation (4) with respect to time we get

$$F_{\rm E+S0} = 1 - [1 - F_0(\Sigma)]e^{-\eta(\Sigma)(t-t_0)}, \tag{5}$$

where $F_{\rm E+S0}$ is the early-type fraction at time t, $F_0(\Sigma)$ is the primordial fraction of early types at a given density, and t_0 is the cluster formation time. This equation can be differentiated to yield

$$\frac{dF_{\rm E+S0}}{dt} = [1 - F_0(\Sigma)]\eta(\Sigma)e^{-\eta(\Sigma)(t-t_0)}. \tag{6}$$

If we assume $\eta(\Sigma) = $ const and $F_0(\Sigma) = 0$, the observed increase in the production rate of early-type galaxies with density suggests that cluster galaxies formed significantly *later* than the field galaxies. Since detailed studies of cluster ellipticals indicate they are older than their counterparts in the field (Bower et al. 1992; Ellis et al. 1997; Stanford et al. 1998; Lucey et al. 1991; van Dokkum & Franx 1996; Bender et al. 1998; Pahre et al. 1998; Kelson et al. 2000), we can rule out differences in formation time as the sole source of the T-Σ relation. A model where $\eta(\Sigma)$ increases with density, but $F_0(\Sigma) = $ const, is also ruled out by the data if we require that formation time is constant or increasing with density. A combination of earlier formation times in dense regions, increasing transformation rates with density, and an intrinsically higher early-type fraction in dense regions is required to explain the observed data with a closed-box model. However, simply allowing for galaxy infall also explains the observed evolution.

Dynamical friction or "harassment" (Spitzer 1958; Moore et al. 1998) is the most likely source of an increased late- to early-type transformation rate in dense regions. This process operates by increasing the orbital energy of stars inside individual galaxies through tidal interactions. The rate of momentum exchange due to dynamical friction increases with density, which naturally leads to the observed increase in transformation rate. Furthermore, Goto (2005) finds differences in the velocity dispersion of cluster early- and late-type galaxies which can be explained if the early-type galaxies underwent more dynamical friction than the late-type galaxies, but cannot be explained by gas stripping. Finally, the amount of energy transferred to a galaxy through dynamical friction is proportional to the galaxy mass (Spitzer 1958; Moore et al. 1998; Goto 2005), so the color-magnitude and fundamental plane relations may also be a consequence.

Intrinsic differences in the galaxy formation process between clusters and the field also appear to be important in determining galaxy morphology. Using only our data, no evolution is measured in the T-Σ relation, but COSMOS only covers redshifts greater than 0.4 and densities $\Sigma < 100$ galaxies Mpc^{-2}. At higher densities, evolution is independently observed by both Smith et al. (2005) and Postman et al. (2005). Nevertheless, the lack of evolution at low densities suggests that the galaxy formation process may be intrinsically different in dense and sparse regions.

Bundy et al. (2006) also find that intrinsic differences in the galaxy formation process may be more important than environment.

They show that the star formation properties of galaxies are more correlated with galaxy mass than environment. Environment is only important when the local galaxy density is significantly greater than the field density. If a similar statement can be made for morphologies, it would explain why evolution is only observed in the highest density regions.

However, morphology and star formation appear to be affected by different processes. The fraction of galaxies with early-type morphologies and the fraction with low star formation rates evolve in different ways with density (see Fig. 13). These different rates of evolution can be explained if the growth in the early-type fraction were driven by interactions, while the reduction in star formation was caused by gas stripping.

Assuming that gas removal due to cluster interactions is responsible for truncating the star formation, we can recycle our closed-box model to describe the process. For the SFR-Σ relation, we get $F_0(\Sigma) = 0$ because stars must form to make galaxies. If the gas density traces the galaxy density, $\eta(\Sigma)$ becomes the rate at which star formation is truncated, and t_0 becomes the formation time for the cluster. This simple model accurately reproduces the observed shape and evolution of the SFR-Σ relation while also predicting reasonable galaxy formation times. However, points at much lower density than what we can probe with photometric redshifts are required in order to confirm the gas striping hypothesis.

Nevertheless, several studies of the local universe also suggest that the SFR-Σ relation is driven by gas stripping, while the T-Σ relation is due to galaxy interactions. Blanton et al. (2005) find that color is a better predictor of density than of morphology, indicating that star formation is strongly affected by environment while early-type morphologies are not necessarily the result of environment. Further evidence is provided by Quintero et al. (2006), who find that both morphology and color are correlated with distance from cluster centers, but that the correlation between morphology and star formation is asymmetric. Specifically, for a given star formation rate, the fraction of morphological early-type galaxies does not change with distance from the cluster, but at a given morphological type, the average star formation rate increases with distance from the cluster. In addition, both Dressler et al. (1997) and Treu et al. (2003) show that morphology is more strongly correlated with local density than distance to the cluster center, indicating that the number of neighbors and hence the number of interactions is the more important quantity in determining morphology.

Galaxy infall may also play a role in shaping the T-Σ relation. It is predicted by CDM models, but it is difficult to explain the small scatter in the colors and fundamental plane of cluster ellipticals if most early-type galaxies were recently transformed from field galaxies. Nevertheless, Treu et al. (2003) point out that the dynamics of galaxy clusters would erase the T-Σ relation if the orbits of individual galaxies were not confined to regions of nearly constant density. So, if infall is responsible, galaxies are likely accreted smoothly via dynamical friction from adjacent regions of already elevated density.

There is no quantitative study of how harassment or gas starvation should affect the evolution of the T-Σ relation. Benson et al. (2001) attempt to model evolution of the T-Σ relation at low densities in CDM simulations via halo mergers. The amplitude of the predicted evolution is correct at $\Sigma = 10$ galaxies Mpc^{-2}, and no differential evolution is seen at lower densities. Unfortunately, at higher densities, where we have the bulk of our data, the Benson et al. model is not valid because individual galaxy orbits are not tracked once the dark matter halos merge; therefore no comparison can be made.

Clearly, more detailed models are needed, but care must be taken when comparing the results. A magnitude-morphology relation is predicted by most CDM models, so changing the magnitude limit used to measure density will change the observed T-Σ relation and its observed evolution. As a result, it is very important to match the absolute magnitude cuts when comparing models and data. Furthermore, the present measurements do not distinguish between moderate density regions on the outskirts of massive clusters and the centers of moderate mass groups. Treu et al. (2003) find that this distinction is not important; nevertheless, it remains a potential source of systematic uncertainty in our measurements.

In considering Figure 11, several limitations of our present data become evident. Our measurement of the early-type growth rate strongly depends on the local measurements from Goto et al. (2003) and Dressler (1980), which use a different morphological classification scheme. Furthermore, the large gap in the data at $0.1 < z < 0.3$, which is nearly a quarter of the cosmic time we probe, limits our ability to measure how the growth in the early-type fraction changes with time. COSMOS has too small an area and the SDSS has neither the depth nor the spatial resolution to probe the T-Σ relation in this gap. To probe a volume at $0.1 < z < 0.3$ comparable to COSMOS at $z = 0.5$, a survey would have to cover $\approx$15 deg^2 with $0.6''$ seeing in one band.

8. CONCLUSIONS

We have developed a technique for measuring the early-type galaxy fraction with density and redshift. The Gini parameter is found to reliably select early-type galaxies with $0.3 < z < 1.2$ using only the ACS F814W filter. This selection is free from systematic effects in redshift (band shifting) or surface brightness.

We find that densities are measurable with photometric redshifts if projected densities are used. Nevertheless, for photometric redshift accuracies of $\Delta_z/(1+z) = 0.03$, projected densities below $\Sigma = 3$ galaxies Mpc^{-2} are difficult to measure. The observed number of galaxies at $\Sigma > 10$ galaxies Mpc^{-2} is significantly higher than that found in earlier CDM galaxy simulations because these simulations did not follow the orbits of galaxies within dark matter halos. The latest simulations now follow galaxies, improving the agreement, but still underestimating the number of galaxies in dense regions.

Using these techniques, we measure the evolution of the T-Σ relation and the growth rate of the early-type fraction with cosmic time. We find that the growth rate of the early-type fraction is increasing with density, which cannot be explained by a closed-box model with early formation times. We conclude that some density-dependent process combined with galaxy infall is responsible for the observed relation and evolution, with dynamical friction and harassment being the most likely mechanisms.

The SFR-Σ relation appears to result from different processes than the T-Σ relation. In particular, the SFR-Σ relation evolves differently from the T-Σ relation, and there does not appear to be a direct relationship between the two. Gas stripping is the most likely source of the SFR-Σ relation.

At $\Sigma = 10$ galaxies Mpc^{-2}, the rate of dark halo interactions in CDM models predicts the correct amplitude of growth in the early-type fraction, but these models are not valid at higher densities. No current model attempts to predict our observed evolution at $\Sigma > 10$, so we can only speculate as to what physical mechanisms must be at play. Furthermore, the current generation of CDM models appears to underestimate the number of galaxies in high-density regions.

We would like to thank Mauro Giavalisco, Jin Koda, and Mara Salvato for their excellent suggestions, feedback, and proofreading; Marc Postman and Graham Smith for providing early preprints of their papers and feedback on this work; Tomotsugu Goto and Andrew Benson for providing data from their figures; and the contributions of the COSMOS team (http://www.astro.caltech.edu/cosmos/). Support for this work was provided by NASA grant HST-GO-09822 and NSF grant OISE-0456439.

REFERENCES

Abraham, R. G., Tanvir, N. R., Santiago, B. X., Ellis, R. S., Glazebrook, K., & van den Bergh, S. 1996, MNRAS, 279, L47
Abraham, R. G., Valdes, F., Yee, H. K. C., & van den Bergh, S. 1994, ApJ, 432, 75
Abraham, R. G., van den Bergh, S., & Nair, P. 2003, ApJ, 588, 218
Abraham, R. G., et al. 2004, AJ, 127, 2455
———. 2007, ApJ, in press (astro-ph/0701779)
Bauer, A. E., Drory, N., Hill, G. J., & Feulner, G. 2005, ApJ, 621, L89
Bender, R., Saglia, R. P., Ziegler, B., Belloni, P., Greggio, L., Hopp, U., & Bruzual, G. 1998, ApJ, 493, 529
Benson, A. J., Frenk, C. S., Baugh, C. M., Cole, S., & Lacey, C. G. 2001, MNRAS, 327, 1041
Bertin, E., & Arnouts, S. 1996, A&AS, 117, 393
Blanton, M. R., Eisenstein, D., Hogg, D. W., Schlegel, D. J., & Brinkmann, J. 2005, ApJ, 629, 143
Bower, R. G., Lucey, J. R., & Ellis, R. S. 1992, MNRAS, 254, 601
Bundy, K., Ellis, R. S., & Conselice, C. J. 2005, ApJ, 625, 621
Bundy, K., et al. 2006, ApJ, 651, 120
Butcher, H., & Oemler, A. 1984, ApJ, 285, 426
Capak, P. 2007, ApJS, 172, 99
Cassata, P., et al. 2007, ApJS, 172, 270
Conselice, C. J., Bershady, M. A., Dickinson, M., & Papovich, C. 2003, AJ, 126, 1183
Cooper, M. C., Newman, J. A., Madgwick, D. S., Gerke, B. F., Yan, R., & Davis, M. 2005, ApJ, 634, 833
Cowie, L. L., Songaila, A., & Barger, A. J. 1999, AJ, 118, 603
Dickinson, M., Papovich, C., Ferguson, H. C., & Budavári, T. 2003, ApJ, 587, 25
Dressler, A. 1980, ApJ, 236, 351
Dressler, A., et al. 1997, ApJ, 490, 577
Drory, N., Salvato, M., Gabasch, A., Bender, R., Hopp, U., Feulner, G., & Pannella, M. 2005, ApJ, 619, L131
Ellis, R. S., Smail, I., Dressler, A., Couch, W. J., Oemler, A. J., Butcher, H., & Sharples, R. M. 1997, ApJ, 483, 582
Ferguson, H. C., et al. 2004, ApJ, 600, L107
Feulner, G., Gabasch, A., Salvato, M., Drory, N., Hopp, U., & Bender, R. 2005, ApJ, 633, L9
Glazebrook, K., et al. 2004, Nature, 430, 181
Goto, T. 2005, MNRAS, 359, 1415
Goto, T., Yamauchi, C., Fujita, Y., Okamura, S., Sekiguchi, M., Smail, I., Bernardi, M., & Gomez, P. L. 2003, MNRAS, 346, 601
Guzzo, L., et al. 2007, ApJS, 172, 254
Hubble, E. P. 1926, ApJ, 64, 321
Juneau, S., et al. 2005, ApJ, 619, L135
Kauffmann, G., White, S. D. M., Heckman, T. M., Ménard, B., Brinchmann, J., Charlot, S., Tremonti, C., & Brinkmann, J. 2004, MNRAS, 353, 713
Kelson, D. D., Illingworth, G. D., van Dokkum, P. G., & Franx, M. 2000, ApJ, 531, 137
Koekemoer, A. M., et al. 2007, ApJS, 172, 196
Lilly, S. J., Le Fevre, O., Crampton, D., Hammer, F., & Tresse, L. 1995, ApJ, 455, 50
Lotz, J. M., Primack, J., & Madau, P. 2004, AJ, 128, 163
Lucey, J. R., Bower, R. G., & Ellis, R. S. 1991, MNRAS, 249, 755
McCracken, H. J., Aussel, H., Capak, P., El-Zant, A., Guzzo, L., & Scoville, N. Z. 2007, ApJS, 172, 314
Melnick, J., & Sargent, W. L. W. 1977, ApJ, 215, 401
Mobasher, B., Capak, P., Scoville, N., Dahlen, T., Salvato, M., Aussel, H., Thompson, D., & Feldman, R. 2007, ApJS, 172, 117
Moore, B., Lake, G., & Katz, N. 1998, ApJ, 495, 139
Oemler, A. J. 1974, ApJ, 194, 1
Pahre, M. A., de Carvalho, R. R., & Djorgovski, S. G. 1998, AJ, 116, 1606
Postman, M., et al. 2005, ApJ, 623, 721
Quintero, A. D., Berlind, A. A., Blanton, M., & Hogg, D. W. 2006, ApJ, submitted (astro-ph/0611361)
Scoville, N. Z., et al. 2007a, ApJS, 172, 150
———. 2007b, ApJS, 172, 38
Smith, G. P., Treu, T., Ellis, R. S., Moran, S. M., & Dressler, A. 2005, ApJ, 620, 78
Somerville, R. S. 2005, in ESO Workshop, Multiwavelength Mapping of Galaxy Formation and Evolution, ed. A. Renzini & R. Bender (Berlin: Springer), 131
Spitzer, L. J. 1958, ApJ, 127, 17
Springel, V., et al. 2005, Nature, 435, 629
Stanford, S. A., Eisenhardt, P. R., & Dickinson, M. 1998, ApJ, 492, 461
Treu, T., Ellis, R. S., Kneib, J., Dressler, A., Smail, I., Czoske, O., Oemler, A., & Natarajan, P. 2003, ApJ, 591, 53
van Dokkum, P. G., & Franx, M. 1996, MNRAS, 281, 985